

Efficient Multi-objective Optimization for Gas Turbine Discs

Francisco Javier Garcia-Revilla, Jesús R. Jimenez-Octavio,
Cristina Sanchez-Rebollo and Alexis Cantizano

Abstract An original multi-objective optimization strategy for aeronautical gas turbine discs is presented in this chapter. A sensitivity analysis together with an optimal design of experiments (DoE) are accomplished prior applying a multi-objective genetic algorithm (MOGA) based on a Kriging surrogate model. Fatigue life prediction and total geometry mass are taken as optimization objectives in this work, whose results can be validated against laboratory tests but going further experimental conditions. To begin with, (i) a first case study considers laboratory test conditions, basically centrifugal loads due to the blades and the own mass of the disc. However, (ii) a second case study considers real conditions such as the centrifugal loads, airflow forces and thermal loads as well as taking into account different typical materials for this application. Results show that the proposed methodology successfully leads to the optimal geometric parameters both for laboratory and real conditions. The main conclusions and qualitative differences are finally summarized, highlighting the suitability of A718Plus among other materials and the *Cob width* parameter as the most critical one.

Keywords Multi-objective optimization · Turbine disc · Design of experiments · Kriging model · Genetic algorithm

F. J. Garcia-Revilla · J. R. Jimenez-Octavio (✉) · A. Cantizano
Department of Mechanical Engineering, Universidad Pontificia Comillas,
c/Alberto Aguilera 25, 28015 Madrid, Spain
e-mail: jesus.jimenez@upcomillas.es

F. J. Garcia-Revilla
e-mail: javier.garcia-revilla@gea.com

A. Cantizano
e-mail: alexis.cantizano@upcomillas.es

C. Sanchez-Rebollo
Institute for Research in Technology, Universidad Pontificia Comillas,
c/Santa Cruz de Marcenado 26, Madrid 28015, Spain
e-mail: cristina.sanchez@iit.upcomillas.es

1 Introduction

Rotating discs are one of the most critical parts of any rotating machinery, thus the optimal design of turbine discs becomes indeed essential for aeroengines [1]. The failure of a disk is absolutely unacceptable due to the hazardous and catastrophic effects that would suffer the engine, airframe, ship or installation if this happens. In order to prevent this fact and achieve an acceptably low probability of individual failure, the discs have very strict design criteria, where the material is carefully selected and stress, thermal, creep, vibration and fatigue analysis have to be satisfied more strictly every day [2].

From the pioneer analytic solutions for rotating discs [3, 4], the significant development in computational continuum mechanics boosts the suitability of much more powerful but computationally expensive techniques like the finite element method (FEM), which really fits from its very beginning the more realistic simulation and design of turbine discs [5–9]. The traditional design process was based on a trial and error method led by a group of experts. Despite the computing capabilities which allow FE simulations, optimal designs were subjected to the same iterative process: searching for the objectives of design but satisfying allowable stress, temperature and fatigue life.

Metaheuristic algorithms are proven to be suitable to tackle multi-objective nonlinear optimization problems, but due to the complexity of gas turbine discs, this may be computationally expensive and almost unapproachable when classic genetic algorithms (GA) are used [10–12]. Shape optimization of the discs used to be the goal when minimum weight designs are intended [13, 14]. However, not only one objective but also two or more can be assumed to lead the optimization process, which requires complementary techniques and sensitivity analysis [15] to simplify the methodology. Thus, simple surrogate models are able to construct an approximate response surface from an initial budget of FE based simulations, which allows optimizing via GA not so costly. Definitely, if the design of experiments (DoE) and the surrogate model are well fitted, a huge amount of FE simulations can be saved within the optimization process. The Kriging method is one of the most extended surrogate models for multidisciplinary optimization [16–18], which has been previously applied to the optimization of turbine discs together with GA, see [19, 20]. In order to save computational costs, even FE analysis can be completely avoided in optimization runs by the coupling of the GA with simplified response surface equations [21].

Furthermore, the selection of the base material is undoubtedly an essential variable of design. Both the mechanical properties and the economic costs are key factors which lead to the optimal design. Nowadays, turbine discs are typically formed from nickel alloy forgings [22]. Due to the high nickel content in its chemistry composition, these nickel-based super alloys present an exceptional combination of mechanical properties like toughness, high temperature strength or resistance to degradation in oxidizing and corrosive environments. They are used widely in aerospace applications and, currently, 40–50 % of the total weight of an

aircraft engine is typically constituted by nickel-based super alloys. More specifically, it is applied in the parts that make up the turbine and the combustion chamber, where the highest operation temperatures are reached and highest loads are suffered.

Avoiding economic criteria, 3 nickel alloys are analyzed in this paper in order to include the material selection in the optimal design. The first one is A718 [23], a nickel based super alloy used extensively in aircraft applications. This alloy has been used for turbine discs for more than 20 years because of its exceptional high temperature mechanical properties. It has excellent strength, hot and cold workability, very good weldability and moderate cost [24]. On the other hand, Waspaloy [25] shows a better weldability and an improved thermal stability but higher economic costs. Likewise, A718Plus [26] is an improved alloy compared with the previous ones. It offers a full 55 °C temperature advantage over A718, maintaining many of the features of it, like good weldability, good workability (even better than Waspaloy), improved thermal stability and moderate cost [27, 28].

Therefore, the goal of this chapter is to state a robust and flexible optimization methodology applied to turbine discs based on low-fatigue life prediction. Basically finding the Pareto front with the optimal solutions which allow the decision maker to quantify the trade-offs in satisfying any different objectives. The optimization objectives herein proposed are the minimization of the geometry mass and the maximization of the fatigue life. The proposal gathers some of the abovementioned techniques, both for the numerical calculation and the optimization process, which provide the backbone of this methodology. A convenient design of experiments and sensitivity analysis prior applying a surrogate model and a multi-objective genetic algorithm is originally applied in this paper, saving huge CPU time. Once any feasible optimal candidate is computed via FEM, computational time becomes a barrier, so the whole method is mainly focused on CPU time saving.

In order to prove the flexibility of the methodology herein proposed, two different cases have been studied: (i) a laboratory based case, whose laboratory test conditions allow the results to be easily checked in a test bench, and (ii) a more realistic case considering flight conditions. This second case includes a specific study on the base material of the rig disc, obtaining promising results. Geometry, loads and boundary conditions are close to real ones, but not exactly due to confidential reasons. Despite this, it is not essential when a methodology is presented, both the degree of complexity of the models and the accuracy of the results are obviously improvable at the expense of the CPU time.

After this brief introduction and review of the state of the art, the paper is organized as follows. [Section 2](#) provides a description of the turbine disc model, details of the cases of study and certain calculation and simulation basis. [Section 3](#) presents the optimization methodology together with its application to the turbine disc model. [Section 4](#) applies the original methodology to the geometry optimization of a test rig turbine disc, used in industry to test the fatigue life of high pressure turbine discs made of A718Plus. [Section 5](#) is an in-depth examination of real operating conditions. Furthermore, the set of materials previously described are herein analyzed. Finally [Sect. 5](#) summarizes the main conclusions of the chapter and highlights the most relevant contributions.

2 Description of the Turbine Disc Model

According to Timoshenko et al. in [3], the most critical part of a rotating disc with hub is located in the inner radius of it. This is also applicable to real operating turbine discs, whose critical part is located also there, in the region commonly called bore. Much effort has been devoted to improve and optimize the bore geometry indeed, assuring that it can resist the typical high stresses of this application. Its geometry is shown in Fig. 1-left.

2.1 Cases of Study

Two different cases are analyzed. In the first case, laboratory isothermal test conditions are considered, that is, the behavior of the rig disc subjected to a Bore Spin Test is studied. The second case seeks to deepen in the methodology herein presented and how it can be applied to real flight conditions and not only to isothermal test conditions. These cases of study are described below.

2.1.1 Laboratory Test Conditions

The rig turbine disc is subjected to a Bore Spin Test carried out by the company Rolls-Royce Deutschland Ltd & Co KG. This test is intended to prove bore lives of the BR725 HP Turbine Stage 1 and 2 as well BR710 HPT Stage 1 (both modern Rolls-Royce Jet Engines) using the material Allvac[®]718PlusTM (A718Plus). The test is also part of a generic spin test program within the frame of the A718Plus material development, and full information about it can be found in [29].

This test is performed by means of spinning the disc at isothermal conditions. Thus, the disc is assembled to a backing disc driven by a shaft. The assembly including both parts is shown in Fig. 1-right.

The assembly has to be cycled from minimum speed to maximum speed and again to minimum speed, with the enough dwell time (2–5 s) at each speed to ensure stable conditions. These cycles are made in two increments: the first one with 25,000 cycles and the second one with 35,000 cycles. After each increment, the disc must be crack tested and also some parts of the disc like the bore, rim or drive arm must be re-measured. These tests conditions are summarized in Table 1.

Results obtained from this test guarantee that the disc would resist real flight speed conditions because the maximum rig speed is much higher than the real aero-engines spin speed (around 15,000 rpm).

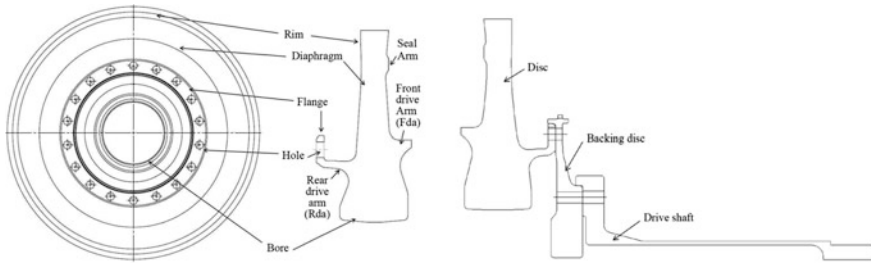


Fig. 1 Turbine disc geometry (*left*) and test assembly including (*right*)

Table 1 Test conditions

Maximum rig speed	21,500 rpm ± 25 rpm
Minimum rig speed	500 rpm ± 50 rpm
Test temperature	430 °C (isothermal) ± 15 °C
Increments	2
First increment	25,000 rig cycles
Second increment	35,000 rig cycles
Total number	60,000 rig cycles

2.1.2 Flight Conditions

A more realistic environment which is closer to real flight conditions is also analyzed. In this study, three different super alloys (A718, Waspaloy and A718Plus) are compared.

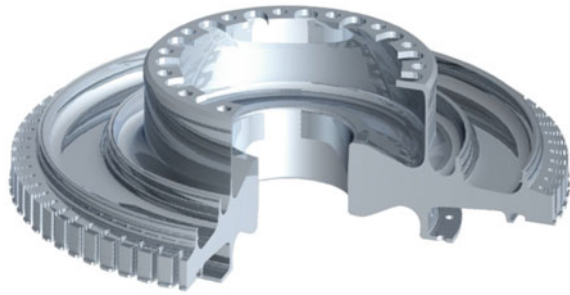
Real temperatures are applied to the disc model and a maximum speed of 1,600 rad/s, which is the maximum taking off speed. Furthermore, the surrogate modeling method is applied to the three proposed materials to check the influence of the material in the shape and mechanical behavior of the disc.

In this second case, the geometry used for the optimization is the same of the previous one. It must be highlighted that a real turbine disc has some features that are not included in this model, like the seals, front and rear drive arms or the multi-lobed roots (commonly named “fir-trees”) used to locate the blades in the rim of the disc. These features can be observed in Fig. 2, where a real high pressure turbine disc is represented. All these elements have an influence on the stress and the temperature distribution of the disc, but these type of rig turbine discs are mainly used for the evaluation of the bore region. Therefore, the results are focused on that part of the model.

2.2 Basic Equations for Stress Calculation

Classic models of axisymmetric discs state the radial and hoop displacements as $\delta = [u, v]^T$, while the strain $\varepsilon = [\varepsilon_r, \varepsilon_\theta, \varepsilon_z, \gamma_{rz}]^T$ and the stress $\sigma = [\sigma_r, \sigma_\theta, \sigma_z, \tau_{rz}]^T$

Fig. 2 High pressure turbine disc geometry



comprise radial, hoop, axial and shearing components. Therefore, the relation between strains and displacements in a turbine disc can be expressed as:

$$[\varepsilon_r, \varepsilon_\theta, \varepsilon_z, \varepsilon_{rz}]^T = \left[\frac{\partial u}{\partial r}, \frac{\partial v}{\partial z}, \frac{u}{r}, \frac{\partial v}{\partial r} + \frac{\partial u}{\partial z} \right]^T$$

While the stress-strain relationship in the disc, assuming thermal and elastic isotropy, is:

$$\begin{bmatrix} \sigma_r \\ \sigma_\theta \\ \sigma_z \\ \tau_{rz} \end{bmatrix} = \frac{E(1-\nu)}{(1+\nu)(1-2\nu)} \begin{bmatrix} 1 & \frac{\nu}{1-\nu} & \frac{\nu}{1-\nu} & 0 \\ \frac{\nu}{1-\nu} & 1 & \frac{\nu}{1-\nu} & 0 \\ \frac{\nu}{1-\nu} & \frac{\nu}{1-\nu} & 1 & 0 \\ 0 & 0 & 0 & \frac{1-2\nu}{2(1-\nu)} \end{bmatrix} \left(\begin{bmatrix} \varepsilon_r \\ \varepsilon_\theta \\ \varepsilon_z \\ \gamma_{rz} \end{bmatrix} - \begin{bmatrix} \alpha\Delta T \\ \alpha\Delta T \\ \alpha\Delta T \\ 0 \end{bmatrix} \right)$$

where E , ν and α denote the Young’s modulus, Poisson’s ratio and thermal expansion coefficient of the material, respectively. Finally T denotes the temperature field in the turbine disc.

The easiest suitable disc shape to analyze without numerical methods is a “coin shape” of constant thickness t , with a hole in the middle, inner radius r_1 and outer radius r_2 , as is shown in Fig. 3-left. In this kind of models, the blade disc rim stress denoted by P_{rim} may be given by the centrifugal pull of the complete blade set divided by the disc perimeter and the thickness.

Assuming tensile plane stress without any thermal load for the sake of clarity and applying equilibrium equations on a differential piece of disc, thanks to Hooke’s law in polar coordinates and certain manipulations it is possible to obtain the following generic solutions of the differential equation for the radial σ_r and hoop σ_θ stresses:

$$\sigma_r = \frac{E}{1-\mu^2} \left(\frac{\partial u}{\partial r} + \mu \frac{u}{r} \right) = \frac{E}{1-\mu^2} \left(C_1(1+\mu) - C_2(1-\mu) \frac{1}{r^2} \right) - \frac{\rho\omega^2}{8} (3+\mu)r^2$$

$$\sigma_\theta = \frac{E}{1-\mu^2} \left(\frac{u}{r} + \mu \frac{\partial u}{\partial r} \right) = \frac{E}{1-\mu^2} \left(C_1(1+\mu) + C_2(1-\mu) \frac{1}{r^2} \right) - \frac{\rho\omega^2}{8} (1+3\mu)r^2$$

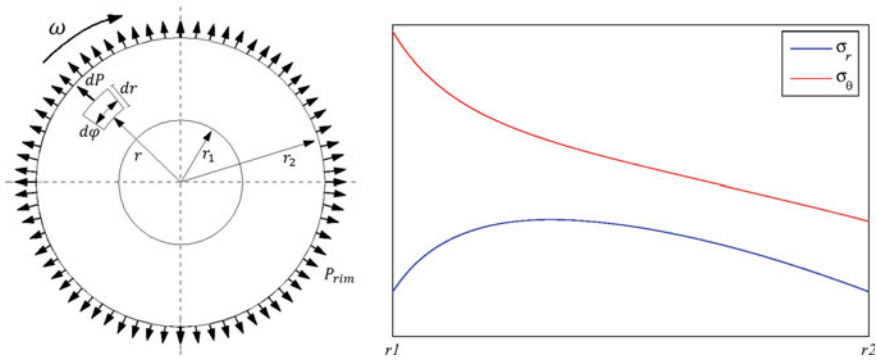


Fig. 3 Differential equilibrium (left) and principal stresses-radius (right)

Boundary conditions on the radial stress allow obtaining the integration constants and the final expressions of radial and hoop stresses are derived and plotted in Fig. 3-right. As it can be deduced from this figure, the most critical part of the disc is located in the position with the smallest radius and corresponds to the hoop stress. This part of the disc is called “cob” and it is strengthened in practice using a wider thickness at this point. Thus the critical hoop stress evaluated in the inner radius is:

$$\sigma_{\theta,crit} = \left(\frac{1 - \mu}{4}\right)r_1^2\rho\omega^2 + \left(\frac{3 + \mu}{4}\right)r_2^2\rho\omega^2 + \frac{2P_{rim}r_2^2}{r_2^2 - r_1^2}$$

Therefore, the results obtained by this classical analysis lead the parameterization and finite element discretization of the computation models used within the methodology herein presented.

2.3 Boundary Conditions and Applied Loads

The dummy blades located in the rim of the rig disc are simulated as a distributed pressure in radial direction. Each dummy blade has a volume of 6,000 mm³ and assuming they are made with the same material A718Plus, each dummy blade has an approximated weight of 49 g. And there are 36 dummy blades. Thus, the following simplified equation reflects the value of the distributed pressure in the rim face P_{rim} ,

$$P_{rim} = \frac{mN\omega^2}{2\pi V4}$$

where N is the number of blades with mass m , ω corresponds to the rotational speed of the disc (in this case fixed at 2251 rad/s) and finally $V4$ is the *Rim width* parameter.

As the backing disc is also subjected to centrifugal forces and it would be deformed with the test rig disc, no restriction to the radial displacement of the flange of the disc is made. On the other hand, axial and transversal displacements remained to be fixed to simulate the transversal influence of the backing disc.

For the second case study, that is, for the flight conditions, different boundary conditions to those for the laboratory test conditions, collected in Table 1, need to be prescribed. In this case, three different temperatures are fixed [30]. It is important to highlight that these temperatures are evaluated in the hottest point of its working cycle; this is during the take-off. This point coincides with the most severe rotating situation due to the turbine disc is also spinning at its highest speed. Therefore, the temperature boundary conditions are:

- 800 °C in the rim zone. This temperature is the highest and it is caused by the hot gases that come from the combustion chamber.
- 700 °C in the front diaphragm zone. Here the cooling air that comes from the compressor is injected in this region in order to cool the blades. This airflow crosses the disc from this area to the rim through a duct that is located under the seals. This temperature is an approximation of the real temperature conditions a real disc can have.
- 600 °C in the bore zone. This part is the coolest of the disc and there are some secondary air flows that refresh this zone by convection.

These temperature gradients are another cause of stress in real turbine discs. This temperature difference is created because the disc does not heat up homogeneously, partly owing to the thick shape of the cob, which takes longer than the rim zone to heat up. Also the previous considerations of the cooling system affect the thermal temperature distribution along the section of the disc. For a typical turbine disc, about 20 % of the bore hoop stress is due to the blades; about 40 % is due to centrifugal.

Also, the rotational speed of the disc has changed to those imposed in the laboratory test conditions gathered in Table 1. This speed is fixed at 1,600 rad/s (15,278 rpm), which despite being slightly lower, it approximately appears during the take-off of the plane and becomes the most critical of all the flight.

2.4 *Finite Element Modeling*

The turbine disc has been modeled with the commercial software ANSYS Workbench as an axisymmetric geometry. A complete axisymmetric geometry using a two-dimensional section has been refused because of the holes for the bolts located in the flange of the disc, but it can be approached as a cyclic axisymmetry configuration. According to this symmetry approach, it is necessary to define the

boundary conditions that indicate which faces corresponds to cyclical geometries repeated 18 times in a polar coordinates system, in order to extrapolate the cyclic behavior.

In Fig. 4, the mesh used to simulate the rig turbine disc is shown, with 42,395 nodes and 24,235 tetrahedral elements within each cyclic section. Special care has been taken with the bore region of the disc detailed in Fig. 4-left, which requires a refinement process to ensure the best possible results in the most critical region.

3 Optimization Methodology

The different steps of the methodology herein presented are described and shown in Fig. 5. In order to fulfill the global objectives which must lead the optimization process, the main parameters of the model which could have significant influence on the optimal design are initially chosen. A design of experiments (DoE) is carried out prior to obtain a response surface by means of the Kriging method, whose fitness quality is conveniently analyzed. These preliminary steps may result crucial for the minimization of the computational cost during the optimization process without giving up accuracy of the solution, which implies a simple iterative process for non-significant parameters removal. Once the design space is obtained, a sensitivity analysis is performed with mid-effects and Pareto charts and, finally, a multi-objective genetic algorithm (MOGA) is applied. With the results obtained, calculation of the fatigue life is carried out.

3.1 Model Parameters

From the detailed description of the rig disc geometry, a reduced set of 16 driving parameters have been taken into account in order to define the general geometry and more precisely its bore region. Thus the optimal design may be classified as sizing and configuration optimization because of the effects derived from the parameterization lead to both kind of changes in the geometry. In Fig. 6, the whole parameterization of the section of the model, with 68 parameters in total, is shown. The varying parameters are highlighted with red circles while the other parameters remain fixed.

The parameters subjected to variation are shown in Table 2. Their codification and name are related to the position they have, depending on the different parts where they are located (rim, bore, diaphragm, drive arm, flange and seal arm). Also identifications about the relative position on the part (rear or front) are provided. Furthermore, the upper and lower limits, as well as their base value are included.

The parameters coded with the letter P are not directly associated with any geometrical measurement. Due to negative dimensions have no sense in a

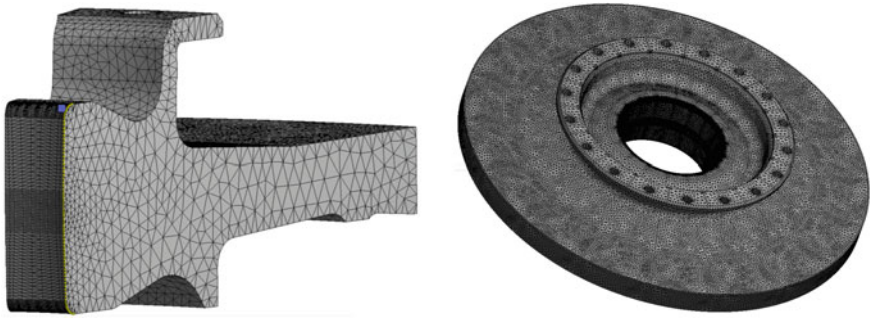


Fig. 4 Detail of the mesh in the bore (left) and whole mesh of the disc (right)

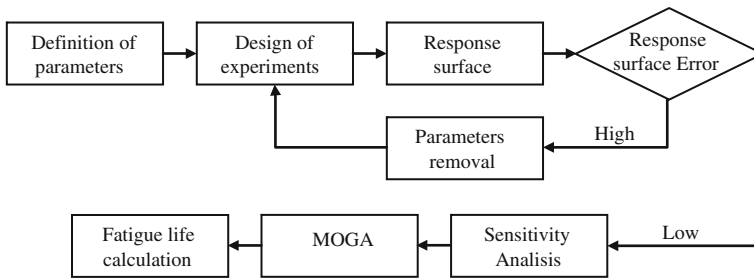


Fig. 5 Flowchart of the optimization methodology

parametric model but some of their basic ranges could include negative values (for example the diaphragm total angle orientation), certain auxiliary parameters that provide the negative varying capability have been added. They are the following:

$$\begin{cases} A83 = A82/2 + P78 \\ V88 = V86 - P84 \end{cases}$$

3.2 Design of Experiments

The sample method selected for the DoE is the Optimal Latin Hyper Cube technique [31]. In this study, each design point corresponds to a certain geometry configuration of the disc. The responses calculated are the two design objectives: geometry mass and critical stress in the bore region. In order to assure the best possible space, all the design explorations are done with 500 runs.

The stress criterion selected is the von Mises one, because it is proportional to the distortion energy. Therefore, it satisfies the property that two stress states with equal distortion energy have an equal von Mises stress. This is why it is considered

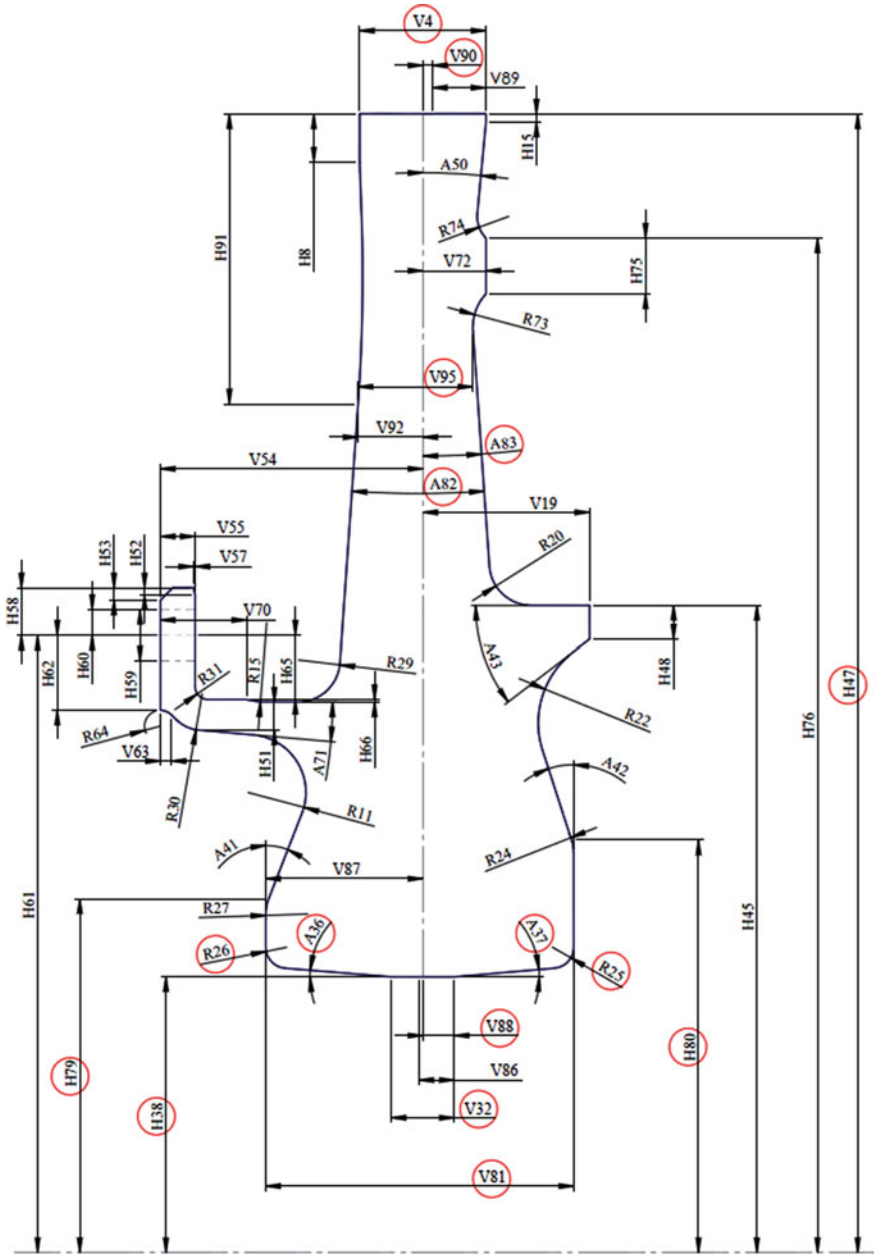


Fig. 6 Parameterization of the disc model

Table 2 Driving parameters of the disc model

Code	Parameter name	Base value	Units	L. limit	U. limit
A36	Cob rear inner angle	2	°	0.1	6
A37	Cob front inner angle	2	°	0.1	6
A82	Diaphragm total angle	8	°	1	10
H38	Cob bore rad.	52.5	mm	40	55
H47	Rim rad.	215.1	mm	213.6	221.6
H79	Cob rear outer dia.	68	mm	62	76
H80	Cob front outer dia.	76.6	mm	68	77
P78	Diaphragm angle aux	0	°	-0.5	1
P84	Cob center line offset	0.05	mm	-2	2
R25	Cob front inner fillet	4	mm	2	6
R26	Cob rear inner fillet	4	mm	2	6
V4	Rim width	24	mm	22.5	25.8
V32	Cob bore length	12	mm	3	15
V81	Cob width	58	mm	48	68
V90	Rim center line offset	1	mm	0	1.8
V95	Diaphragm width	20	mm	17.5	21

a very good measurement for ductile materials, such as metals, as the onset of yield for these materials does not depend on the hydrostatic component of the stress tensor and so it is a good average for the whole stress behavior of the disc.

3.3 Evaluation of the Response Surface Error and Parameters Removal

In order to analyze which are the most relevant parameters and which of them are statistically negligible, estimated parameters are reported for each response (critical stress and geometry mass). This analysis sorts all the different parameters, computing the estimates of each of them with the help of the design exploration data. These estimates can be easily compared using the t-ratio as a coefficient of the estimate and the standard error given by the distribution for each of the parameters. The result of this comparison is sorted by the absolute value of the t-ratio and with significance level of 0.05 and those non significant parameters are eliminated

3.4 Sensitivity Analysis

As it was previously mentioned, the use of Kriging surrogate models to calculate the regression-based interpolation of the response surface makes it possible to get better results for the approximation [32]. There have been used 34 refinement points in the Kriging algorithm in order to obtain a predicted relative error lower

than 5 % in the surface, which can be considered good enough for this analysis. Also the calculation of the surface includes 5 verification points to confirm that the model really corresponds to the real behavior of the disc. Once the response surface has been calculated, it is possible to obtain results and conclusions.

The influence of each variable in the system is analyzed with main-effects charts for each of the responses, critical stress and geometry mass, for a better understanding of the whole system. Also, using a Pareto chart, all the variables are sorted by their influence on the response, providing as well quadratic and cross effects between parameters. This chart complements the conclusions that can be obtained from the main-effects chart allowing a deeper understanding of the behavior of the system.

3.5 Multi-objective Genetic Algorithm

Once the response surface has been calculated, a MOGA algorithm can be applied in order to obtain the optimal candidates of the problem [33]. Without loss of generality of the optimization methodology, two objectives lead the optimal designs in this work: the minimization of the geometry mass [34] and the maximization of fatigue life. Assuming simplified models, the second one may be considered inversely proportional to the critical stress, so the minimization of the stress becomes definitively the second optimization objective although the fatigue life is post-processed.

Pareto fronts are the most extended chart to depict the feasible region and the frontier of optimal design points when multi-objective optimization is performed. Once the process is leaded by antagonistic objectives, Pareto front becomes a very helpful tool for the decision maker due to its quantitative and qualitative representation of the non-dominated optimal candidates. The NSGA-II [35] multi-objective genetic algorithm has been applied due to its well known advantages when obtaining the Pareto fronts. This algorithm starts with 2,000 initial samples and each of its subsequent iterations continues with 1,000. The maximum allowable Pareto percentage was chosen as 55 %. This value can set the selection pressure of each one of the iterations. It is recommended to use values between 55 and 75 %. Finally, 50 iterations are set as the maximum allowable the algorithm can do.

4 Case Study I: Results for Laboratory Test Conditions

Regarding the laboratory test conditions detailed in Sect. 2.1, this section presents the results obtained step by step along the whole optimization process: (i) the evaluation of the response surface error and parameters removal, (ii) the sensitivity analysis, (iii) the results provided by the multi-objective genetic algorithm NSGA-II and, finally, (iv) the fatigue life calculation.

4.1 Evaluation of the Response Surface Error and Parameters Removal

In order to analyze which are the most relevant parameters and which of them are statistically negligible, estimated parameters are reported for each response (critical stress and geometry mass). Thus, these are sorted by the absolute value of the t -ratio, showing the most significant effects at the top. Also a bar chart is provided, which shows the t -ratio, with lines showing the 0.05 significance level. In each of these tables, Prob > | t | column indicates the significance. Values with *-symbol beside them are p -values, i.e. the results which are statistically significant.

Initially, all the parameters are included in the model; therefore the first DoE explores 16 variables along 500 different design points. The results obtained in this analysis correspond to Tables 3 and 4. On the other hand, the created response surface has a global error of 129 %. This value is so high due to the elevated number of input parameters the system has. If no parameters removal would be wanted, more than 500 design points will be needed, but this becomes computationally unviable.

Comparing these two tables, it can be noted that the parameters *Cob rear inner fillet*, *Diaphragm angle aux*, *Cob front inner fillet*, *Cob center line offset* and *Rim center line offset* appear in both tables in the least relevant positions in the effect scale. This scale, corroborated by the p -values for each of the parameters allows depreciating these 5 parameters and removing them from the model, making them fixed at their base point value in further analysis. Also, it can be seen that the critical stress response only has in this analysis 2 statistically significant parameters, meanwhile the geometry mass has 7 parameters. This can be explained because the direct relationship that can be found between part dimensions and volume and hence also between dimensions and geometry mass.

This process is repeated until all the remaining parameters are relevant to explain the behavior of the system and the modeled response surface error is low enough to assure that it has been calculated properly. Tables 5 and 6 show the 6 parameters that left over after the iteration. In these two tables, it can be seen how all the remaining parameters have p -values statistically relevant for the geometry mass and 5 from 6 parameters in the critical stress. Also, the non-relevant parameter from this table has a p -value (0.069) really close to the significance level (0.05). Furthermore, it must be highlighted that all the remaining parameters correspond to the dimensions that roughly define the geometry (inner and outer diameters of the disc) or the widths of its most main parts (rim, cob and diaphragm). Moreover, the global error of the response surface calculated is 4.91 % which is low enough to assure correct and robust results.

According to these results, it can be concluded that the model has been cleaned from all the non-relevant parameters assuring a better optimization process as the model is simpler and also a better sensitivity analysis as all the parameters included in the model have relevance.

Table 3 Sorted parameter report for critical stress with 16 parameters

Parameter name	Estimate	Std error	t ratio	Prob > t
Cob width	-71429681.41	10821541.4	-6.6	<0.0001*
Cob rear outer dia.	-33141292.15	14758667.5	-2.25	0.0252*
Rim width	81782593.09	62510369.3	1.31	0.1914
Cob bore length	22385702.96	17168116.8	1.3	0.1929
Rim rad.	33203157.79	25853572.9	1.28	0.1997
Cob rear inner angle	-42823606.73	34869406.6	-1.23	0.22
Diaphragm total angle	-27738496.55	23160651.5	-1.2	0.2317
Cob front outer dia.	-24002510.8	22870002.7	-1.05	0.2945
Cob bore rad.	-12096135.83	13612280.5	-0.89	0.3747
Cob front inner angle	27210008.78	34902522.3	0.78	0.436
Rim center line offset	-74961854.05	114771615	-0.65	0.514
Cob center line offset	-22847704.25	51418346.2	-0.44	0.657
Cob front inner fillet	-22328215.39	51073482.2	-0.44	0.6622
Diaphragm angle aux	-58035858.21	137764042	-0.42	0.6738
Diaphragm width	9787156.128	58548133.5	0.17	0.8673
Cob rear inner fillet	-5.74E + 06	52142124.8	-0.11	0.9125

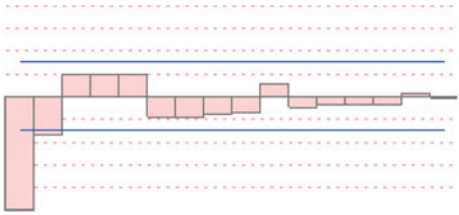


Table 4 Sorted parameter report for geometry mass with 16 parameters

Parameter name	Estimate	Std error	t ratio		Prob > t
Cob width	0.01126099	0.0006442	17.48		<0.0001*
Cob bore rad.	-0.00734693	0.00081033	-9.07		<0.0001*
Rim rad.	0.01329415	0.00153904	8.64		<0.0001*
Diaphragm width	0.02749039	0.00348532	7.89		<0.0001*
Diaphragm total angle	0.01074019	0.00137874	7.79		<0.0001*
Cob rear outer dia.	0.00592983	0.00087857	6.75		<0.0001*
Rim width	0.01431233	0.00372119	3.85		0.0001*
Cob front outer dia.	0.00262273	0.00136143	1.93		0.0547
Cob bore length	-0.00099901	0.001022	-0.98		0.3288
Cob front inner angle	-0.00126635	0.00207772	-0.61		0.5425
Cob rear inner fillet	0.00135929	0.00310398	0.44		0.6616
Cob center line offset	0.00048174	0.00306089	0.16		0.875
Diaphragm angle aux	0.0008143	0.00820099	0.1		0.9209
Cob rear inner angle	-0.0001941	0.00207575	-0.09		0.9255
Cob front inner fillet	-5.1942E-05	0.00304036	-0.02		0.9864
Rim center line offset	5.61E-06	0.00683226	0		0.9993

Table 5 Sorted parameter report for critical stress with 6 parameters

Parameter name	Estimate	Std Error	t Ratio		Prob > t
Cob width	-6440130.05	317733.92	-20.27		<0.0001*
Rim rad	8927804.42	789722.809	11.3		<0.0001*
Diaphragm total angle	-6450075.26	702999.878	-9.18		<0.0001*
Rim width	9831053.4	1917882.53	5.13		<0.0001*
Cob bore rad	2117015.63	421877.418	5.02		<0.0001*
Diaphragm width	3294740.53	1808070.66	1.82		0.069

Table 6 Sorted parameter report for geometry mass with 6 parameters

Parameter name	Estimate	Std Error	t ratio		Prob > t
Cob width	0.0115767	9.4105E-05	123.02		<0.0001*
Cob bore rad	-0.0079035	0.00012495	-63.25		<0.0001*
Rim rad	0.01396832	0.0002339	59.72		<0.0001*
Diaphragm width	0.03026036	0.00053551	56.51		<0.0001*
Diaphragm total angle	0.00967198	0.00020821	46.45		<0.0001*
Rim width	0.01487849	0.00056803	26.19		<0.0001*

4.2 Sensitivity Analysis

The sensitivity analysis herein presented uses a Kriging model to simulate the behavior of the system. A predicted relative error in the surface of 4.9162 % is

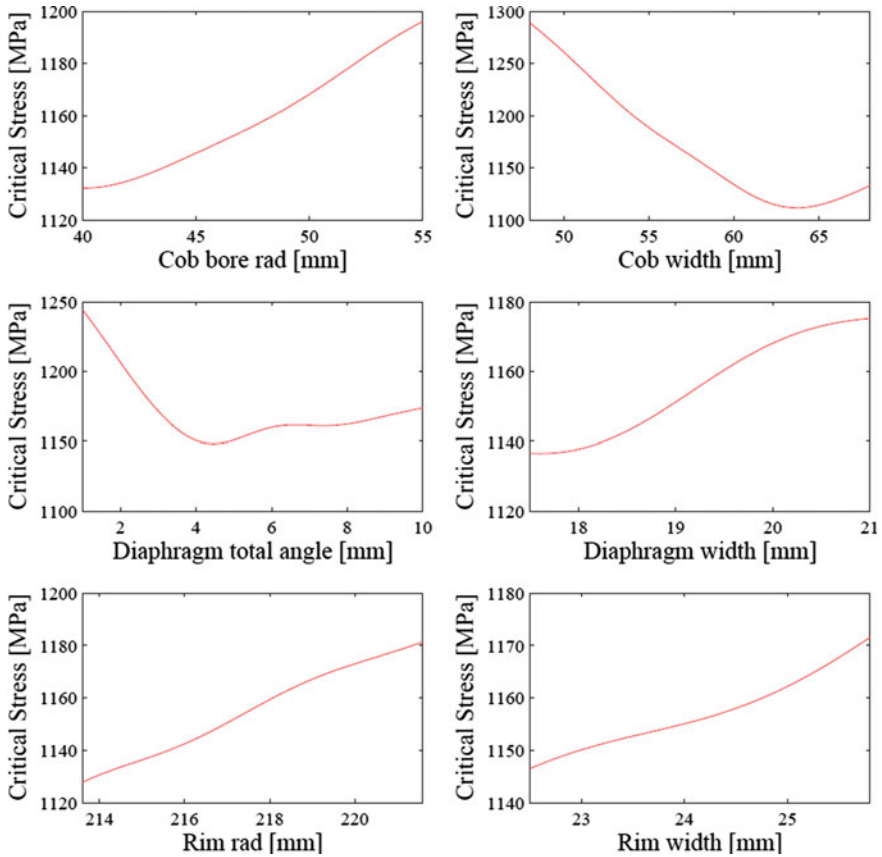


Fig. 7 Critical stress individual parameter responses of the disc

considered accurate enough for this analysis. So, once the response surface has been calculated, it is possible to obtain results.

The individual response of each of the parameters when the other parameters are fixed is firstly presented in Figs. 7 and 8. This allows obtaining a preliminary idea about how the system can be optimized according to the individual effect of each parameter.

In Fig. 7 the individual response to the critical stress of the disc of the 6 remaining parameters are shown. The represented responses model the individual behavior of each of the parameters supposing the other ones fixed at their medium value of each range of variation. It can be seen in this figure how the *Cob bore rad*, *Diaphragm width*, *Rim rad* and *Rim width* parameters have a strictly increasing shape, while the *Cob width* and *Diaphragm total angle* parameters have a minimum in the middle of their range of variation. These results are very useful to understand how the critical stress behaves with the variation of each parameter.

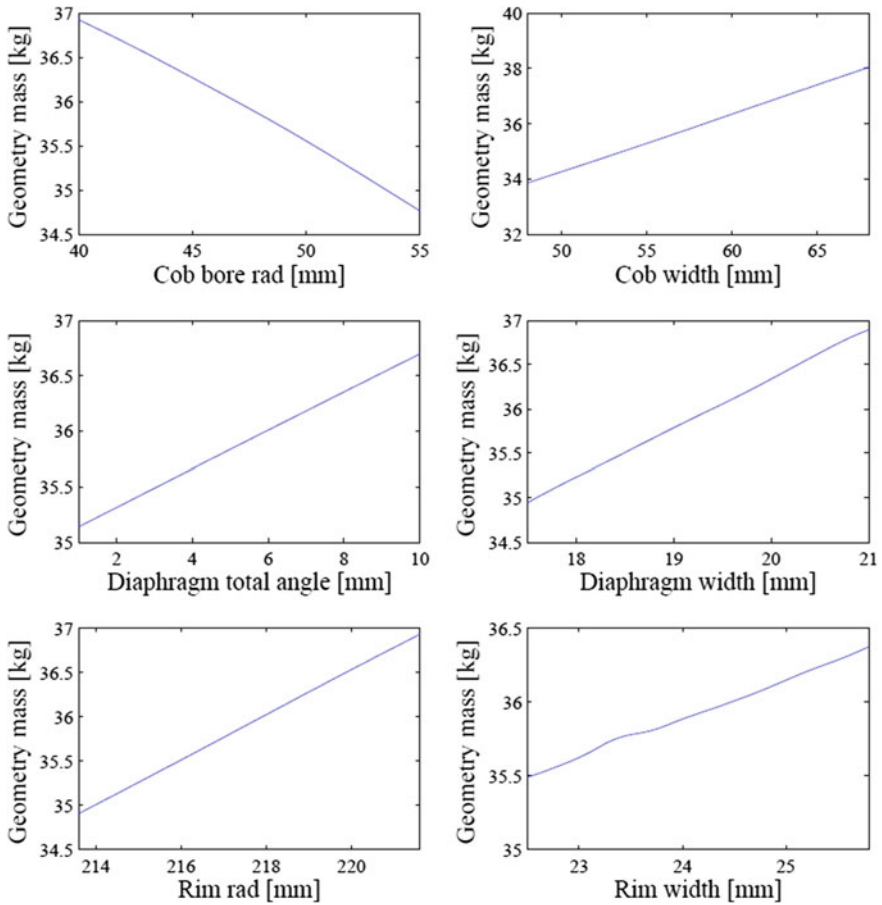


Fig. 8 Geometry individual parameter responses of the disc

Alternatively, the geometry mass responses of all the parameters are shown in Fig. 8. At first glance, it is possible to note that all of them have quasi-linear behavior in contrast to critical stress responses. This is explained because all the variation ranges of the parameters correspond to linear or quasi-linear dimensions in the model such as distances or angles, thus the influence on the volume and hence on the mass is linear and the responses show straight lines. Note the parameters related to radius, *Cob bore rad* and *Rim rad*, should obviously lead to a quadratic effect on the geometry mass unless the variation range is so small that it seems quasi-linear indeed. Furthermore, *Cob bore rad* is the only parameter with a decreasing shape. This coincides logically to the definition of this dimension that corresponds to the inner radius of the disc, and thus its increase causes directly mass growth.

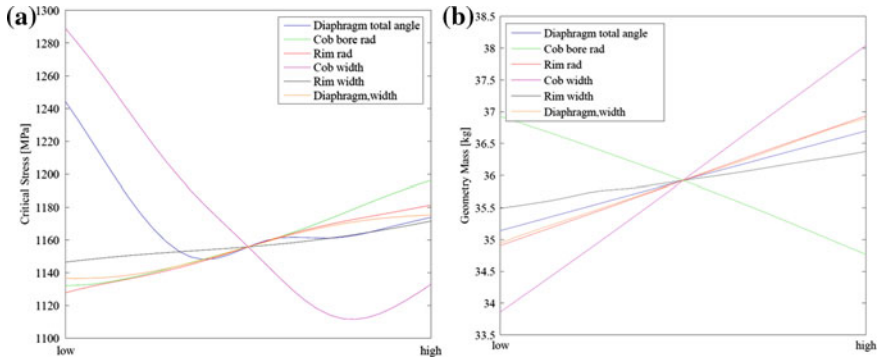


Fig. 9 Main-effects chart applied to critical stress and geometry mass

These results allow seeing separately the influence of each variable in the system but, a better understanding of the whole system can be reached using the main-effects charts for each of the responses (critical stress and geometry mass). Analyzing the main-effects chart it is possible to join all the previous responses and observe which are the most influential and the approximated consequences that would carry out varying one or other parameters.

In Fig. 9a, b can be found the main-effects chart applied to the critical stress and geometry mass of the disc, respectively. As it is shown, in both charts the most influential parameter is the *Cob width* of the disc. It must be reminded that all the plots cut each other in the middle point of their range because every parameter is evaluated remaining the others fixed at their medium value.

This analysis is extended by means of Pareto charts which show not only the influence of the variation of a parameter individually but also the combination of parameters or quadratic variation. Interesting results can be obtained from the response surface by means of these Pareto charts. Firstly, the one represented in Fig. 10 sorts the influence of the parameters in the critical stress response of the disc system. It only includes the effects that have greater influence than 1 %, so only 80 % of the whole response is represented in the chart. Thus the remaining 20 % corresponds to effects with negligible effects. It can be noted that *Cob width* is the parameter that affects to the critical stress the most. This corroborates what was deduced with the main-effects chart applied also to the critical stress.

In Fig. 11 the Pareto chart applied to the geometry mass response is provided. As well as in the previous chart, there are only effects represented with an influence greater than 1 %. In contrast to the critical stress Pareto chart, 84 % of the whole response can be explained with the simple parameters due to their quasi-linear behavior. Therefore, according to the ranking most part of the geometry mass can be explained just with simple terms.

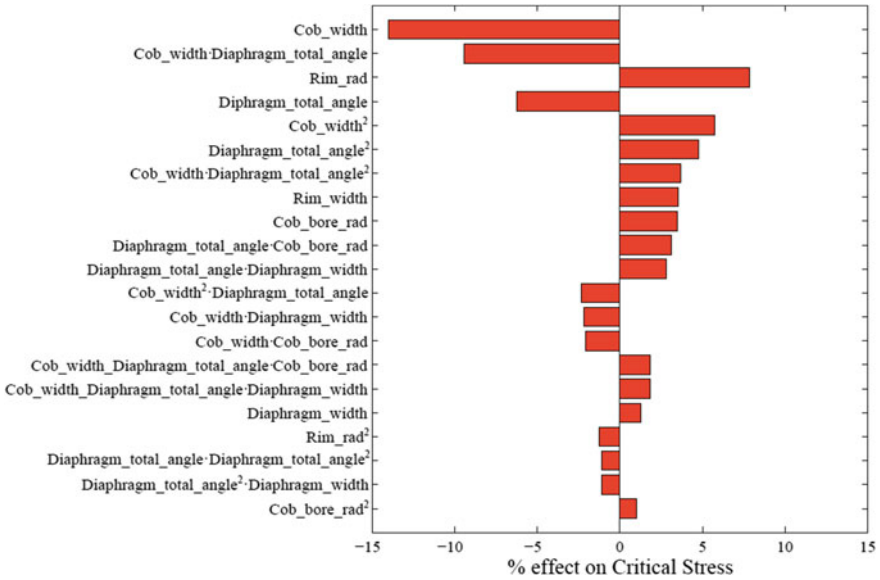


Fig. 10 Pareto chart applied to critical stress of the disc

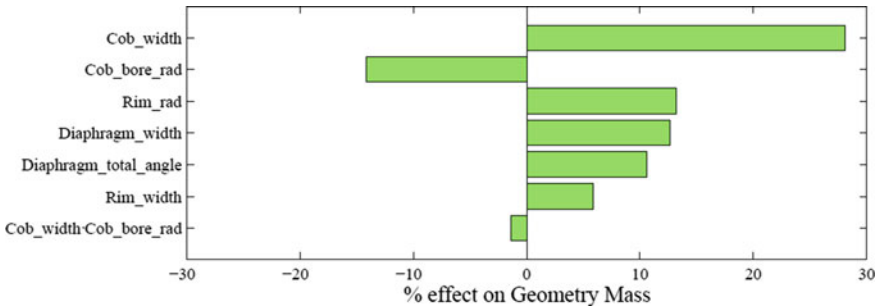


Fig. 11 Pareto chart applied to geometry mass of the disc

4.3 Multi-objective Optimization

Once the response surface has been calculated, it is possible to apply the MOGA algorithm in order to obtain the optimal candidates of the problem.

According to the reference values reported in Sect. 3.5, Fig. 12 shows the Pareto front obtained after the optimization calculation is done. In this chart, all possible candidates are shown gathered in a single Pareto front. As it was explained previously, all these design points are the set of non-dominated optimum values of the system.

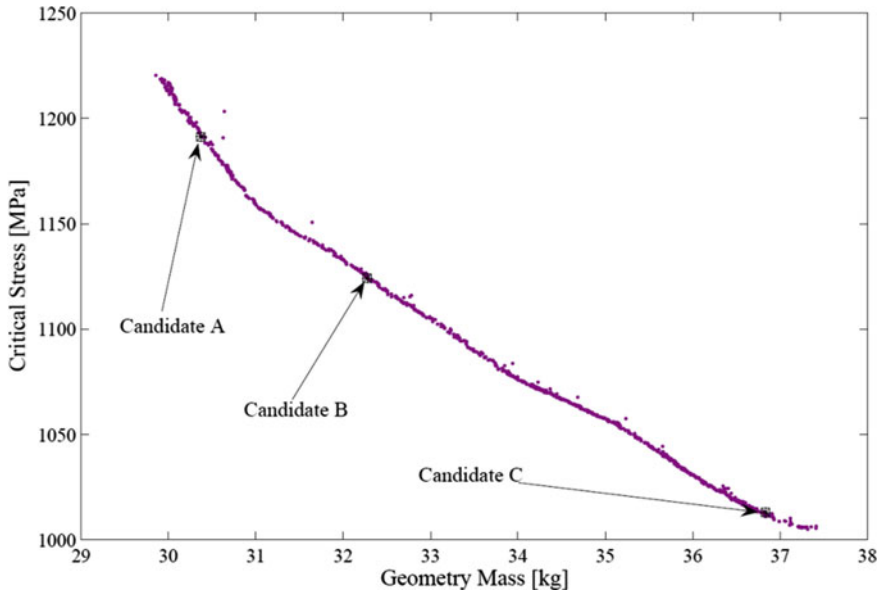


Fig. 12 Pareto front chart of the disc optimization with optimal candidates

Due to the shape of the front, which does not provide clearly any region of dominance, no point of the front could be selected a priori as a candidate suiting better both objectives. Therefore three candidates are selected from this Pareto front and they are proposed as Candidates A, B and C to the global optimum. On the one hand Candidate A has critical stress reduction priority while Candidate C has geometry mass reduction priority, and on the other hand, Candidate B is more balanced geometry mass reduction and critical stress reduction.

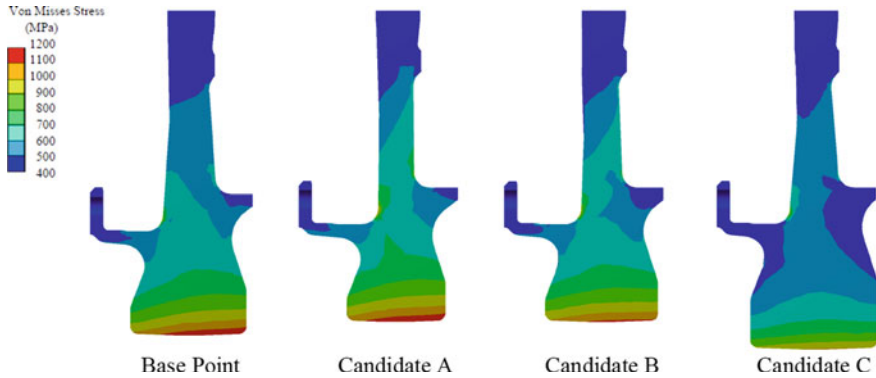
The following Table 7 shows the values of all the relevant driving parameters for each of the candidates proposed, strongly validating the conclusions obtained by means of the sensitivity analysis.

It can be observed how the most varying parameter is the *Cob width* of the disc. This corresponds to its key role in the Pareto charts (Figs. 10 and 11). On the other hand, *Rim width* parameter remains almost fixed in the three candidates, which can be also explained by the Pareto charts. The rest of the parameters follow similar tendencies, although they are not so strongly correlated with the previous sensitivity analysis as the *Rim width* and *Cob width*.

In Fig. 13 the different stress states of the candidates are shown in contrast to the base design point. In this figure, it can be appreciated how the critical stress zone remains being in the cob of the disc, which is consistent with the results obtained from the Pareto front. The shape of the stress distribution is symmetrical with respect to its middle line and also it must be highlighted the existence of a loaded zone in the fillet between the rear drive arm and the diaphragm, but the values of stress in this area are considerably lower than the ones obtained in the

Table 7 Parameter values for the optimal candidates of the disc optimization

Parameter name	Units	Candidate A	Candidate B	Candidate C
Diaphragm total angle	°	1.19	4.47	9.34
Cob bore rad.	mm	54.70	54.73	40.47
Rim rad.	mm	213.60	213.61	213.62
Cob width	mm	50.63	57.93	65.33
Rim width	mm	22.51	22.52	22.51
Diaphragm width	mm	17.52	17.52	17.53

**Fig. 13** Optimal candidates and base design point stress comparison

bore, thus this will never be a critical zone. Also it can be noted in this figure that Candidate A shows the thinnest shape, being the angle of the diaphragm and the width of the cob very small in contrast to the other candidates. On the contrary, Candidate C has larger volume and hence it is heavier too. Also it must be highlighted the smaller value of the radius of the cob, which is considerably lower than the other two candidates. On the other hand, Candidate B presents an intermediate value of cob width and diaphragm total angle which makes possible the balance between mass and stress as it was expected.

4.4 Fatigue Life Calculation

Once the stress distribution of the rig disc, material properties and load cycles are known, it is possible to calculate the fatigue life of each of the candidates. This purpose requires information about the curve alternating stress–life and uses the correction factors which take into account physical differences between the theoretical test specimen and the real part. The stress–life curve is created with and the actual designed part. According to [36], the correction factors are the following:

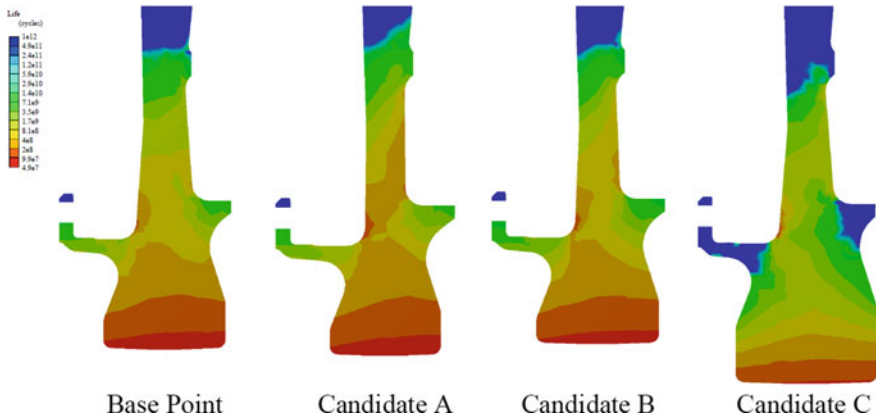


Fig. 14 Optimal candidates and base design point life comparison

$$\begin{aligned}
 C_{load} &= 1.00 \\
 C_{size} &= 0.60 \\
 C_{surf} &= 0.86 \\
 C_{temp} &= 1.00 \\
 C_{reliab} &= 0.90
 \end{aligned}$$

By means of these coefficients, the global fatigue coefficient which allows calculating the expected life of each one of the candidates, depicted in Fig. 14, is:

$$K_f = C_{load}C_{size}C_{surf}C_{temp}C_{reliab} = 0.46$$

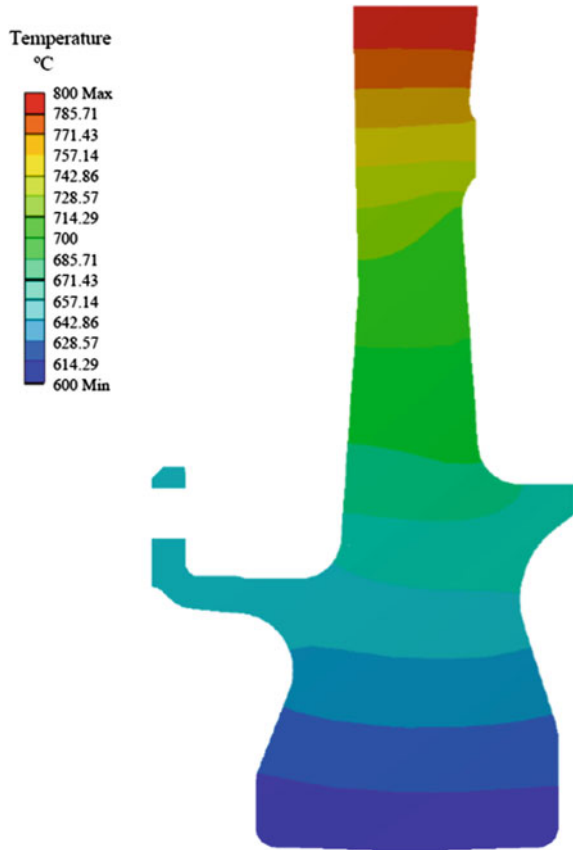
The life shape of all the models is closely connected with the stress shape of Fig. 13, where the stress distribution is shown. Obviously the life of the disc is function of the alternating stress the part suffers, which lead to similar diagrams.

All the previous results (geometry mass, critical stress and fatigue life) of each one of the candidates and the base point are summarized in the following Table 8. In spite of the base geometry for the turbine disc, the loads and boundary conditions are not exactly real due to confidential reasons. It is noteworthy that the expected life for the three candidates are really close to real ones according to the feedback from industry.

Table 8 Optimization results

	Base point	Candidate A	Candidate B	Candidate C
Geometry Mass (kg)	35.38	30.40	32.29	36.82
Critical Stress (MPa)	1188.8	1193.2	1126.9	1020.2
Life (cycles)	51 328 000	49 527 000	61 035 000	85 583 000

Fig. 15 Temperature distribution along the disc section



5 Case Study II: Results for Flight Conditions

This second case study seeks to deepen in how the methodology herein presented can be applied under real conditions and not only under isothermal test conditions. Therefore this part of the study looks to give a more realistic environment, closer to real flight conditions. In addition, this study intends to analyze the suitability of three typical turbine discs super alloys.

According to the flight boundary conditions pointed out in [Sects. 2.1](#) and [2.3](#), herein the results obtained within the optimization process are presented. Once the most severe thermal distribution under the abovementioned conditions is reached, depicted in [Fig. 15](#), the evaluation of the response surface error and parameters removal together with a sensitivity analysis has been carried out.

As well as the previous Case Study I, each one of the materials (Waspaloy, A718 and A718Plus) has been subjected to a design exploration process. The results obtained show that the relevant parameters are exactly the same as the ones from the Bore Spin Test conditions with A718Plus, see [Tables 3](#) and [4](#). Therefore,

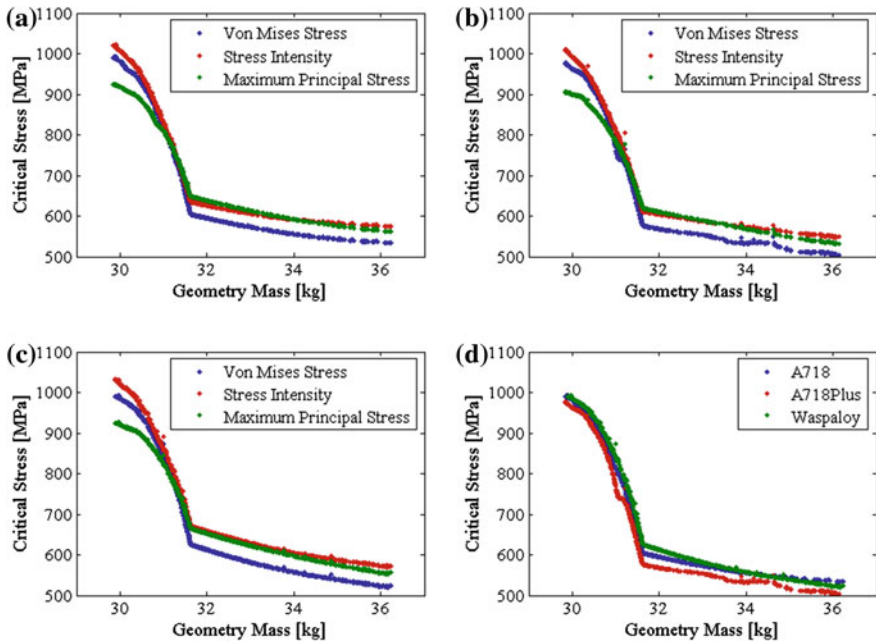


Fig. 16 Pareto fronts of material comparison. **a** A718 **b** Waspaloy **c** A718Plus **d** Von Mises Stress

the most relevant parameters to the critical stress and geometry mass of the disc are not case-dependent. Thus, each one of the material-based cases of study is evaluated with the final 6 critical parameters obtained for the Case Study I and gathered in Tables 5 and 6.

The response surface for each of the material-based cases is calculated using the Kriging method once again. The thermal influence is added as another input but maintaining 500 points of design in the DoE, so the global error of the response surface increases slightly to 5.5 % approximately for each case. In spite of this, this value is low enough to assure that the response surface is able to provide accurate and reliable results.

5.1 Multi-objective Optimization

After calculating the three response surfaces for each of the materials, it is possible to apply the MOGA optimization method to obtain the Pareto front with the optimal candidates. These Pareto fronts are shown in Fig. 16.

In this figure, each of the materials is evaluated separately, taking into account three different stress criteria. The shape of the diagram shows that for every criterion, there is a design point more likely to be the global optimum of the

Table 9 Parameters values for optimal candidates

Parameter name	Units	A718	Waspaloy	A718Plus
Diaphragm total angle	°	1.0023	1.0007	1.0023
Cob bore rad.	mm	40.0011	40.0001	40.0037
Rim rad.	mm	213.6020	213.6031	213.6020
Cob width	mm	48.0027	48.1307	48.0050
Rim width	mm	22.5008	22.5008	22.5008
Diaphragm width	mm	17.5000	17.5006	17.5009

system. This is the corner where the curves change their curvature. Also it is possible to see that in this point the most restrictive criterion is the von Mises equivalent stress. A preliminary way to compare which of the materials is the best option for a turbine disc is observing these Pareto fronts and comparing them for the same stress criterion. For that reason Fig. 16d presents a comparison among the three materials when the von Mises equivalent stress is one of the optimization criteria. As it can be seen the A718Plus curve remains at lower values of geometry mass and critical stress than Waspaloy and A718.

Thus the points located in the corner of the Pareto fronts for each of the materials are assumed as optimum candidates and their values are gathered in Table 9. Due to the geometry design is not material-dependent, the optimal geometry can be reached by means of any alloy. Therefore, the only way to choose the optimal material lies in the comparison of the different stress distributions keeping the geometry mass constant.

Figure 17 shows the stress distribution along the section of the disc for each of the materials in the optimum design point. Although results are quite similar, A718Plus leads to lower values of the von Mises equivalent stress in the bore, which is definitively the critical zone. This agrees that A718Plus is a refined alloy that improves the material properties of Waspaloy and A718, being more adequate for this application thanks to its consequent longer fatigue life.

5.2 Fatigue Life Calculation

The stress distribution allows calculating the fatigue behavior of the part using also the alternating stress—life curve and the correction factors previously mentioned. In this Case Study II, the only parameter that varies from the previous case is the C_{temp} , which swaps from 1.00 to 0.42, because it is evaluated taking into account the real environmental temperature approximated to 550 °C. According to previous considerations, the global fatigue coefficient is:

$$K_f = C_{load}C_{size}C_{surf}C_{temp}C_{reliab} = 0.19$$

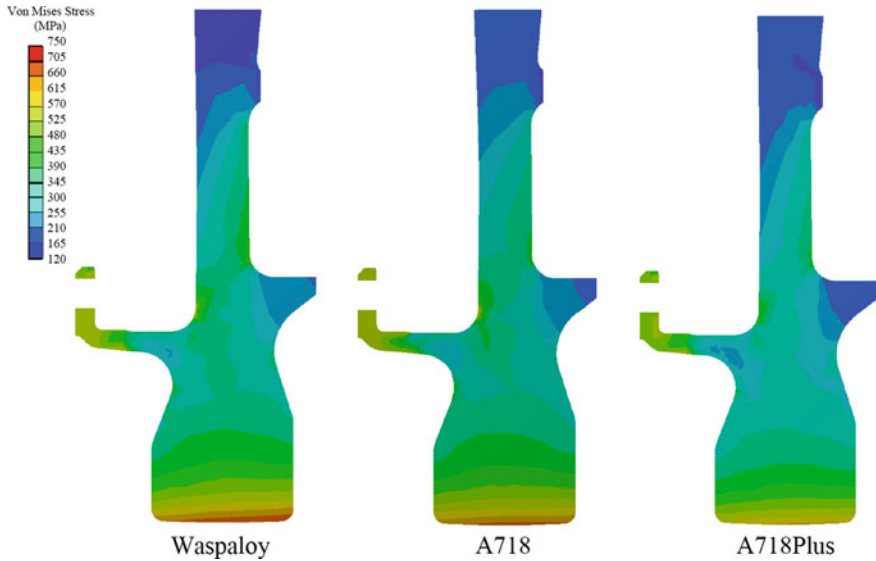


Fig. 17 Stress distribution comparison for the different materials

Table 10 Case study ii optimization results

	Waspaloy	A718	A718Plus
Geometry Mass (kg)	31.62	31.62	31.62
Critical Von Mises stress (MPa)	631.10	611.94	581.67
Life (cycles)	∞	∞	∞

The results obtained in the fatigue life calculation reveal that all candidates present infinite life for the stress and conditions proposed in this case study. This corresponds to real design criteria that states that the critical parts cannot fail under any working circumstances due to the dangerous effects this could lead to.

All the previous results are summarized in Table 10, where the optimal design objectives obtained for each different material are collected. Once again A718Plus excels the other materials owing to its lower critical von Mises stress despite the fact that its geometry mass is exactly the same as the others.

6 Summary and Conclusions

This chapter presents a robust and flexible optimization methodology for turbine discs based on low-fatigue life prediction. Sizing and configuration optimal designs are performed according to two leading objectives: the minimization of the geometry mass and the maximization of fatigue life, which means definitively the minimization of the critical stress.

The methodology herein proposed iteratively gears an initial design of experiments with a sensitivity analysis and a surrogate model prior to run the multi-objective genetic algorithm. The greatest advantage of this procedure is the CPU time saving, but also it includes an accuracy improvement due to the non-significant parameters removal. The purging of non-feasible and non-relevant optimal solutions step by step becomes the main feature of this method and has revealed crucial to perform precise FEM computations of the thermo-mechanical model.

The results obtained in Case Study I, for laboratory test conditions, and Case Study II, for flight conditions, allow highlighting two main conclusions: (i) the *Cob width* parameter of the turbine disc is the most influential in the optimal design and (ii) the super alloy A718Plus evidences much better behavior than super alloys A718 and Waspaloy when realistic flight conditions are considered within the optimization process.

Acknowledgements The authors gratefully acknowledge the technological support of Rolls-Royce in Germany.

References

1. Witek, L.: Failure analysis of turbine disc of an aero engine. *Eng. Fail. Anal.* **13**(1), 9–17 (2006)
2. Rolls-Royce (2005) *The Jet Engine*
3. Timoshenko, S.P., Goodier, J.N.: *Theory of Elasticity*, 3rd edn. McGraw-Hill, New York (1970)
4. Leopold, W.: Centrifugal and thermal stresses in rotating disks. *ASME J. Appl. Mech.* **18**, 322–326 (1984)
5. Meguid, S.A., Kanth, P.S., Czekanski, A.: Finite element analysis of fir-tree region in turbine discs. *Finite Elem. Anal. Des.* **35**(4), 305–317 (2000)
6. Farshi, B., Jahed, H., Mehrabian, A.: Optimum design of inhomogeneous nonuniform rotating discs. *Comput. Struct.* **82**(9–10), 773–779 (2004)
7. Ranta, M.A.: On the optimum shape of a rotating disk of any isotropic material. *Int. J. Solids Struct.* **5**, 1247–1257 (1969)
8. Luchi, M.L., Poggialini, A., Persiani, F.: An interactive optimization procedure is applied to the design of gas turbine discs. *Comput. Struct.* **11**, 629–637 (1980)
9. Chem, J.M., Prager, W.: Optimal design of rotating disk for given displacement of edge. *J Optimiz Theory App* **6**, 161–170 (1970)
10. Genta, G., Bassani, D.: Use of genetic algorithms for the design of rotors. *Meccanica* **30**(6), 707–717 (1995)
11. Tiwari, B.R., Rao, R.: Optimum design of rolling element bearings using genetic algorithms. *Mech. Mach. Theory* **42**(2), 233–250 (2007)
12. Feng, F.Z., Kim, Y.H., Yang, B.: Applications of hybrid optimization techniques for model updating of rotor shafts. *Struct Multidiscip O* **32**, 65–75 (2006)
13. Silva, D.: Minimum weight design of disks using a frequency constraint. *J Eng Ind* **91**, 1091–1099 (1969)
14. Cheu, T.: Procedures for shape optimization of gas turbine. *Comput. Struct.* **54**, 1–4 (1990)
15. Shu-Yu, W., Yanbing, S., Gallagher, R.H.: Sensitivity analysis in shape optimization of continuum structures. *Comput. Struct.* **20**, 855–867 (1985)

16. Simpson, T.W., Mauery, T.M., Korte, J.J., et al.: Kriging models for global approximation in simulation-based multidisciplinary design optimization. *AIAA J* **39**(12), 2233–2241 (2001)
17. Huang, D., Allen, T.T., Notz, W.I., et al.: Sequential Kriging optimization using multiple-fidelity evaluations. *Struct Multidiscip O* **32**(5), 369–382 (2006)
18. Sakata, S., Ashida, F., Zako, M.: On applying Kriging-based approximate optimization to inaccurate data. *Comput Methods Appl M* **196**(13–16), 2055–2069 (2007)
19. Song, W., Keane, A.J.: An efficient evolutionary optimisation frame-work applied to turbine blade fir tree root local profiles. *Struct Multidiscip O* **29**, 382–390 (2005)
20. Huang, Z., Wang, C., Chen, J., et al.: Optimal design of aeroengine turbine disc based on Kriging surrogate models. *Comput. Struct.* **89**, 27–37 (2011)
21. Mohan, S.C., Maiti, D.K.: Structural optimization of rotating disk using response surface equation and genetic algorithm. *Int J Comput Methods Eng Sci Mech* **14**(2), 124–132 (2013)
22. Boyce, M.: *Gas Turbine Engineering Handbook*. Butterworth-Heinemann, Elsevier, Oxford (2006)
23. ATI Allvac (2012) ATI 718™ Alloy
24. Pollock, T.M., Tin, S.: Nickel-based superalloys for advanced turbine engines: chemistry, microstructure, and properties. *J. Propul. Power* **22**(2), 361–374 (2006)
25. ATI Allvac (2011) ATI Waspaloy Alloy
26. ATI Allvac (2004) ATI 718Plus Alloy
27. Uzunonat, Y., Cemal, M., Cevik, S. et al.: Allvac 718Plus™ superalloy for aircraft engine applications (2012)
28. Jeniski, R.A., Kennedy, R.L.: *Development of ATI Allvac 718Plus Alloy and Applications* (2011)
29. Rolls-Royce Deutschland Ltd & Co KG (2011) Test Requirement Document for Bores Spin Test SP.190 in A718Plus
30. Buschoff, T., Voigt, M., Chehab, E. et al.: *Probabilistic Analysis of Stationary Gas Turbine Secondary Air Systems*, GT2006-90261, Barcelona (2006)
31. Wang, G.: Adaptive response surface method using inherited Latin hypercube design points. *J. Mech. Des.* **125**(2), 210–220 (2003)
32. Forrester, A.I.J., Keane, A.J.: Recent advances in surrogate-based optimization. *Prog Aerospace Sci* **45**(1–3), 50–79 (2009)
33. Kessler E, van Houten MH (2007) *Multidisciplinary Optimisation of a Turbine Disc in a Virtual Engine Environment*. 2nd European Conference for Aerospace Sciences (EUCASS), Amsterdam
34. Jahed, H., Farshi, B., Bidabadi, J.: Minimum weight design of inhomogeneous rotating discs. *Int J Pres Ves Pip* **82**(1), 35–41 (2005)
35. Deb, K., Pratap, A., Agarwal, S., et al.: A fast and elitist multiobjective genetic algorithm: NSGA-II. *IEEE T Evolut Comput* **6**(2), 182–197 (2002)
36. Norton, R.L. *Machine design: an integrated approach*. Vol. 3. New Jersey: Pearson Prentice Hall, (2006)